# Construction of biomimetic catalysis system coupling polyoxometalates with deep eutectic solvents for selective aerobic oxidation desulfurization

Mingyue Chi[a], Zhiguo Zhu[a],*, Lulu Sun[a], Ting Su[a], Weiping Liao[a], Changliang Deng[a], Yuchao Zhao[b], Wanzhong Ren[b], Hongying Lü[a],*

[a] Green Chemistry Centre, College of Chemistry and Chemical Engineering, Yantai University, 30 Qingquan Road, Yantai 264005, Shandong, China
[b] Collaborative Innovation Center of Light Hydrocarbon Transformation and Utilization, College of Chemistry and Chemical Engineering, Yantai University, 30 Qingquan Road, Yantai, 264005, Shandong, China

A B S T R A C T

Designing green and efficient catalytic system under extremely mild conditions with high atom economy is always desired in practical applications. In this study, an innovative and efficient biomimetic catalytic system coupling polyoxometalate (POM, Anderson-type $Na_3H_6CrMo_6O_{24}$) with deep eutectic solvents (DESs) is proposed. This coupled system is applied for oxidation desulfurization, which exhibited extraordinary desulfurization performances at the extremely low temperature of 60 °C with the ambient pressure using oxygen as the oxidant. The desulfurization process follows the extraction-oxidation mechanism, during which POM severed as the electron transfer mediator is essential for highly efficient aerobic oxidation desulfurization. The deactivation of this catalytic system after reuse for four times was likely derived from the transformation of $Na_3H_6CrMo_6O_{24}$ POM crystal structure. In addition, the incomparable desulfurization performances of this biomimetic system in commercially available diesel further strongly confirm the potential application on an industrial scale. More importantly, this work is helpful in the precisely design and development of biomimetic coupled systems for catalytic applications under extremely mild conditions.

## 1. Introduction

Sulfur oxide ($SO_x$) exhausted from automotive emission has become a significant concern for worldwide countries in the present time, which not only contributes to irreversible poisoning of noble metal catalyst in the automobile exhaust gas converter but also corrodes engine in company with the decrease of service life [1,2]. Additionally, this kind of oxide gas is also capable of bringing about environmental pollution issues such as acid rain, haze, and so on [3,4]. Considering these drawbacks, numerous countries put forward stringent national requirements to reduce the sulfur contents in fuel oil, which is the main origin of $SO_x$ [5,6]. For example, China has taken actions to enact the Chinese National V Standard, trying to reduce the sulfur content in oils below to 10 ppm [7]. Therefore, the deep desulfurization for fuel oil is an urgent need to obtain extremely low, even free, S-containing oil.

Significant efforts, including hydrodesulfurization [2,8], adsorptive desulfurization [1], extractive desulfurization [9], and oxidation desulfurization [3,4], have been made to address the sulfur content issue in diesel and gasoline. Among these processes, a mature technique, hydrodesulfurization (HDS), is widely employed to remove sulfur compounds in fuel oil *via* a hydrogenolysis route in practical industry process nowadays. This process is usually performed at high temperature (300–500 °C) and pressure (30–70 at m.) with noble metal based catalysts, which naturally leads to the disadvantages of security threat, high cost, and great energy consumption [10]. The sulfur-containing compounds in diesel and gasoline primarily consist of thiophene, benzothiophene (BT), dibenzothiophene (DBT), and their derivatives, which are not easily removed by hydrodesulfurization due to the existence of stable C-S conjugated system in thiophene ring [11]. Moreover, the 4,6-dimethyldibenzothiophene (4,6-DMDBT) is more difficult to be converted than other sulfides on account of the steric hindrance from substituent groups [12]. On the other hand, although adsorptive and extractive desulfurization can remove sulfide in fuel oil to some extent, the deep desulfurization was not able to be achieved [1,9]. Both the approaches cann't satisfy the requirements of sulfur contents in the final products.

As an alternative route for desulfurization, oxidation desulfurization (ODS) is highly efficient for sulfide removal, in particular for thiophene-corresponding such as DBT and aromatic sulfur compounds [13]. These heterocyclic sulfides can be oxidized to polar sulfones, subsequently

---

which are easily eliminated by extraction or adsorption. Unlike HDS, it is under mild conditions that ODS is usually carried out, along with the preponderance of low energy consumption and cost [3,4,13]. Many groups attempted to perform this ODS process with different types of oxidants such as organic peroxyacid, hydrogen peroxide, $NO_2$, $O_2$, and so on [5,14]. Among them, the utilization of $O_2$ as oxidant is highly desirable due to the fact that no by-products is generated in the whole process with high atomic economy [15]. Besides, this process is also green, safe, and inexpensive. Numerous kinds of catalysts, consisting of metal oxide [16], carbon nanometer tube [17], metal organic framework [18], and graphene oxide [19], were reported to be employed in the aerobic oxidation desulfurization (AODS). The common issue is that the present AODS processes are taken with a sacrificial agent or at relatively high temperature and pressure because of the low activity of $O_2$ [16–19]. In a previous work, we found that Anderson-type polyoxometalate, possessing a central metal-oxygen octahedron surrounded by six edge-sharing metal-oxygen octahedron and redox property, demonstrated unique desulfurization performances without the assistance of any sacrificial agents using $O_2$ as oxidant at the temperature of 80 °C [20,21]. The main drawback of this system was the difficulty in recycling and separation, which motivated us explore an innovative route to address this issue coupled with further decreasing the reaction temperature.

Very recently, deep eutectic solvents (DESs) has been paid great attention owing to their cheap and biodegradable properties, which are formed by hydrogen bond between a hydrogen bond acceptor (HBA) and a hydrogen bond donor (HBD) [22]. They have been used in the desulfurization process, but not the desired AODS probably resulting from the high activation energy of $O_2$.

It is well-established that peroxyorganic acids such as peroxyorganic sulfonic acids are highly effective oxidants for ODS [23,24]. However, they are difficult to obtain through the direct oxidation of organic acid by $O_2$ under mild conditions. In the nature or human body, it is found that the aerobic selective oxidation process is common under extremely mild conditions, even at the room temperature. The organics with high energy is unable to be directly oxidized by $O_2$, but indirect oxidation is realized *via* an electron transfer mediator (ETM). The whole oxidation process involves several interconnected redox cycles, giving the decrease of activation energy [25,26]. Inspired by this, the polyoxometalate has determined to be an ETM for transferring electron during the AODS process [15]. However, the structure-activity relation and the practical role of the ETM were still indistinct and the deep insight understanding on biomimetic process for AODS is highly desired.

With the purpose to realize deep desulfurization of diesel under mild conditions, an innovative biomimetic system coupling polyoxometalate with DES was proposed in this manuscript. Decalin was employed as the solvent of model diesel oil, which was intensively reported in literatures [4,5,16]. Both the composition of DES and polyoxometalate played a considerable role in the removal of S-containing compounds, which functioned synergistic effect. Additionally, it was under extremely more mild conditions (60 °C, atmospheric pressure, $O_2$ as the oxidant) that this desulfurization process was implemented in comparison to other present desulfurization system. The textural properties of $CrMo_6$ polyoxometalate and DES as well as catalytic reaction mechanism were systematically studied *via* a series of characterization techniques. Moreover, this biomimetic desulfurization route was also highly efficient for sulfur removal to commercially available diesel, confirming its robust desulfurization performances.

## 2. Experimental section

### 2.1. Materials

The following chemicals were used as provided without further purification: 5-sulfosalicylic acid (99%, Macklin), salicylic acid (99.5%,

Macklin), *p*-amino salicylic acid (98%, Macklin), 3, 4-dihydroxybenzoic acid (97%, Macklin), oxalate dihydrate (AR, Sinopharm Chemical Reagent Co., Ltd), DL-malic acid (99%, Sinopharm Chemical Reagent Co., Ltd), polyethylene glycol 2000 (PEG2000, AR, Macklin), sodiummolybdate sodium ($Na_2MoO_4$, 99%, Macklin), chromium nitrate ($Cr(NO_3)_3$, AR, Sinopharm Chemical Reagent Co., Ltd), tetradecane (98%, Aladdin), 1-benzothiophene (BT, 97%, Macklin), dibenzothiophene (DBT, 98%, Macklin), 4,6-dimethyldibenzothiophene (4,6-DMDBT, 98%, Sinopharm Chemical Reagent Co., Ltd), decalin (GR, Sinopharm Chemical Reagent Co., Ltd), commercially available diesel (Commercial Diesel I and II, purchased from China Petroleum & Chemical Corporation).

### 2.2. Preparation of DESs

PEG2000 was utilized as the HBA. Simultaneously, one type of organic acids, including 5-sulfosalicylic acid (SSA), salicylic acid (SA), *p*-amino salicylic acid (PAS), 3, 4-dihydroxybenzoic acid (DHBA), oxalate dihydrate (OXA), and DL-malic acid (DL-MA), was chosen as the HBD. DES was readily prepared by mixing the HBA and HBD under suitable conditions. In a typical run, PEG was uniformly mixed with HBD such as SSA in a round-bottomed flask at a PEG/HBD molar ratio of 2, and then this mixture was stirred vigorously in an oil bath at the temperature of 80 °C. After the homogeneous liquid was formed, the as-synthesized DES was obtained, denoted as PEG/SSA. With respect to other five kinds of HBD, the prepared procedure was the same to PEG/SSA system. And the corresponding product was designed as PEG/SA, PEG/PAS, PEG/DHBA, PEG/OXA, and PEG/DL-MA, respectively.

### 2.3. Synthesis of $Na_3H_6CrMo_6O_{24}$ polyoxometalate

$Na_3H_6CrMo_6O_{24}$ polyoxometalate was synthesized in our laboratory according to procedures reported previously with minor modification [27]. Typically, $(NH_4)_2MoO_4$ (7.25 g) was slowly added into 15 mL deionized water and then this solution with the pH of 4.5 adjusted *via* aqueous $HNO_3$ (65 wt %), denoted A solution, was stirred vigorously at 45 °C. On the other hand, 2 g of $Cr(NO_3)_3$ was introduced into 2 mL deionized water, giving B solution. Subsequently, B solution was dropwise added into A solution, forming C solution, under stirring, during which the color of this suspension liquid changed from violet to red. Followed by this, the filter liquor, obtaining from filtration of C solution, was refluxed for 10 min at 120 °C and then was maintained at the room temperature for $3 - 5$ days to make product crystallized. Finally, the as-synthesized sample, designated as $CrMo_6$ POM, was withdrawn from the synthesis mixture by filtration, dried at 60 °C for 24 h under vacuum condition.

### 2.4. Characterizations

The X-ray diffraction (XRD) patterns were obtained using a Rigaku Smart Lab3 X-ray diffractometer with Cu-K$\alpha$ radiation ($\lambda = 1.5405$ Å) at 35 kV and 25 mA. UV–vis (UV–vis) diffuse reflectance spectra were performed on a TU-1901 spectrophotometer using $BaSO_4$ as the reference in the region of 200–800 nm. FT-IR spectra were collected using KBr pressuring method on a Shimadzu IRAffinity-1S FT-IR spectrometer in transmittance mode at a spectral resolution of 4 $cm^{-1}$. Conductivity was measured on a DDS-302 conductivity meter, while viscosity was carried out utilizing DV2T viscometer. X-ray photoelectron spectroscopic (XPS) analyses were performed on a AXIS-ULTRA DLD-600W spectrometer equipped with a monochromatized aluminum X-ray source. The analysis data were calibrated using C 1s band at 284.5 eV as the internal standard of binding energy.

### 2.5. Catalytic reactions

Firstly, the model diesel, containing one kind of BT, DBT, or 4,6-

DMDBT, with the sulfur content of 500 ppm was prepared as follows. A certain amount of S-containing compound was dissolved in decalin solvent with the tetradecane of 2000 ppm as internal standard (After evaluation, the decalin and tetradecane were stable in the following oxidation reaction.). Then this mixture was transferred into 1000 mL volumetric flask, the volume of which was maintained to 1000 mL.

The desulfurization performance of extraction and aerobic oxidative desulfurization (EAODS) was tested in a 100 mL round-bottomed flask connected to a water condenser under appropriate stirring. In a typical run, model diesel prepared above (S content of 500 ppm, 20 mL) and DES (4 mL) were stirred in the flask at 333 K for 30 min in the first stage of extraction desulfurization (EDS). Then $CrMo_6$ POM (0.02 g) synthesized above was added into the mixture with the $O_2$ flow rate of 60 mL $min^{-1}$. Meanwhile, the reaction system was timed and analyzed the S content in the upper oil phase at various times. The sample was centrifuged and analyzed using a gas chromatograph (FuLi 9750, FID detector) equipped with a 50 m HP-5 capillary column to obtain the conversion and selectivity. The products were identified on a GC–MS (Agilent-6890GC/5973MS).

The sulfur removal was determined from the following criteria, S removal $= \frac{n_S^0 - n_S}{n_S^0} \times 100\%$, where $n_S^0$ and $n_S$ stand for initial and final mole content of sulfur-containing compounds, respectively.

Note that this EAODS catalytic system (*i.e.*, PEG/SSA and $CrMo_6$ POM system) was also applied to two kinds of commercially available diesel, including Commercial Diesel I and II. The DES of 10 mL and practical diesel of 10 mL was added into the reaction system. Other procedures were the same to that for model diesel. The sulfur content was analyzed using microcoulometry (RPA-100, Jianghuan Analytical Instrument Co., Ltd) coupled with GC-FPD (Agilent 7890B; HP-5 capillary column, 50 m; FPD) to determine sulfur removal performance.

## 3. Results and discussion

### 3.1. Characterizations of $CrMo_6$ polyoxometalate

$CrMo_6$ polyoxometalate was readily crystallized under mild conditions, whose structure was identified by various techniques in the following parts. FT-IR was first applied to characterize the structure of as-prepared polyoxometalate (Fig. 1A). It gave a series of peaks associated with Mo-O-Mo vibration (576, 641, and 786 $cm^{-1}$), Mo = O structure (892, 923, and 948 $cm^{-1}$), and Cr-O vibration (418 $cm^{-1}$) [20,28], indicating that $CrMo_6$ sample possessed a Anderson-type structure. XRD is a common method to detect crystal structure such as zeolites, metal oxide, polyoxometalate [29]. As shown in Fig. 1B, some characteristic and intensive peaks of $CrMo_6$ sample were clearly observed at $2\theta$ = 10.6, 15.7, 16.9, 21.9, 31.2, and 44.5°, which were in line with Anderson-type polyoxometalate (JCPDS No. 28-1092). Meanwhile, as can be seen from UV–vis spectrum (Fig. 2), a broad and intensive adsorption band in the region of 211–330 nm was obviously

demonstrated, resulting from ligand-to-metal charge transfer from an $O^{2-}$ to an $Mo^{6+}$ ion in a octahedral configuration [20]. It also exhibited two relatively weak and broad peaks centred at 400 and 541 nm, attributed to $Cr^{III}$-O structure [30].

The chemical composition of $CrMo_6$ sample was determined from ICP technique. After analysis, the molar ratios of Na/Cr and Mo/Cr were 3 and 6, respectively, further confirming that the chemical formula of $CrMo_6$ sample was $Na_3H_6CrMo_6O_{24}$. It is generally recognized that the micro-environment of chemical element in polyoxometalate is closely related to its catalytic performance [31,32]. XPS is an effective technique for investigating the existing states of ions in polyoxometalate [13,15,20]. Thus, the Cr 2p, Mo 3d, and O 1s XPS spectra were performed to detect chemical state of corresponding element (Figs. 3 and S1). Obviously, this $CrMo_6$ sample was mainly composed of Cr, Mo, and O elements, consistent with the results of ICP. Subsequently, the original XPS spectra for each element were deconvoluted into several peaks. With respect to Cr element (Fig. 3A), two signal bands at around 577.3 and 587.2 eV, attributed to $2p_{3/2}$ and $2p_{1/2}$ photoelectrons of $Cr^{3+}$ species, respectively [33], were observed. Similarly, it also showed $Cr^{4+}$ (578.8 and 588.3 eV) and $Cr^{6+}$ (581.3 and 590.4 eV) species [33,34]. The results indicated Cr element existed in the form of $Cr^{3+}$, $Cr^{4+}$, and $Cr^{6+}$ three states. For Mo species (Fig. 3B), Mo 3d XPS spectra exhibited two peaks at about approximate 232.5 and 235.7 eV, ascribed to $3d_{5/2}$ and $3d_{3/2}$ photoelectrons of $Mo^{6+}$ ions, respectively [20,35]. It was inferred that the Mo element in this $CrMo_6$ sample possessed sole one species ($Mo^{6+}$ species). As elucidated in Fig. S1 (Supporting Information), 530.3, 531.6, and 533.3 eV photoelectrons peaks, associated with Mo-O, Cr−OH, and adsorbed $H_2O$, respectively [36], were clearly noticed.

At this point, conclusion could be made that the prepared $CrMo_6$ polyoxometalate was highly crystallized with Anderson-type structure, as shown in Scheme 1. Mo micro-environment in this sample was uniform, giving rise to exclusive $Mo^{6+}$ species.

### 3.2. Characterizations of DESs

DESs are extensively applied to series of fields such as organic synthesis, electrochemistry, and catalysis as green solvents due to easy preparation, low-cost raw materials, environmentally friendly process, and so on [22,37,38]. Before adopting them to EAODS system, physicochemistry properties (*i.e.*, conductivity and viscosity) of DESs were investigated. The conductivities of six DESs, including PEG/SSA, PEG/SA, PEG/PAS, PEG/DHBA, PEG/OXA, and PEG/DL-MA, were measured at 60 °C. As depicted in Fig. 4A, the conductivity for PEG/SSA DES (50.7 μs $cm^{-1}$) was considerably superior to these for other ones (a similar level below 10 μs $cm^{-1}$). It was speculated that this phenomenon was probably due to the discrepant chemical composition, in particular the functional groups. There is no denying that mobility rate for charge carrier is tightly associated with liquid conductivity [39].
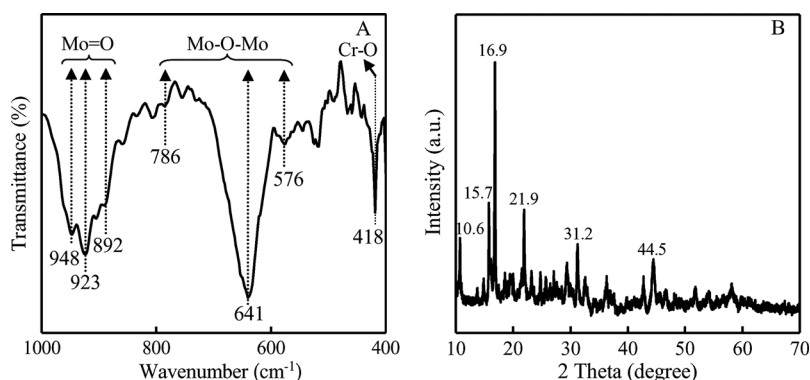


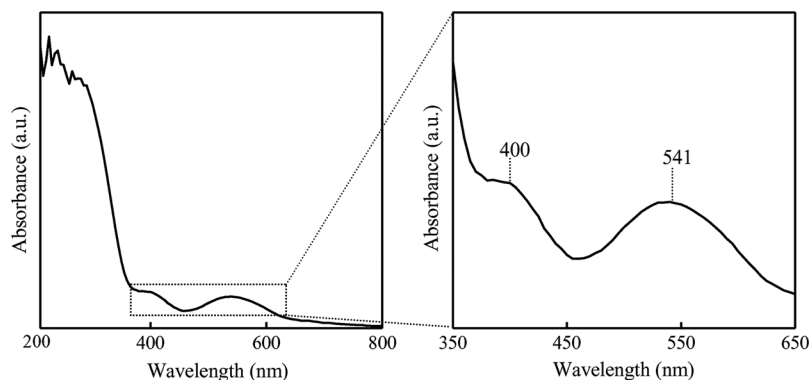**Fig. 1.** (A) FT-IR spectrum and (B) XRD pattern of prepared $Na_3H_6CrMo_6O_{24}$ sample.
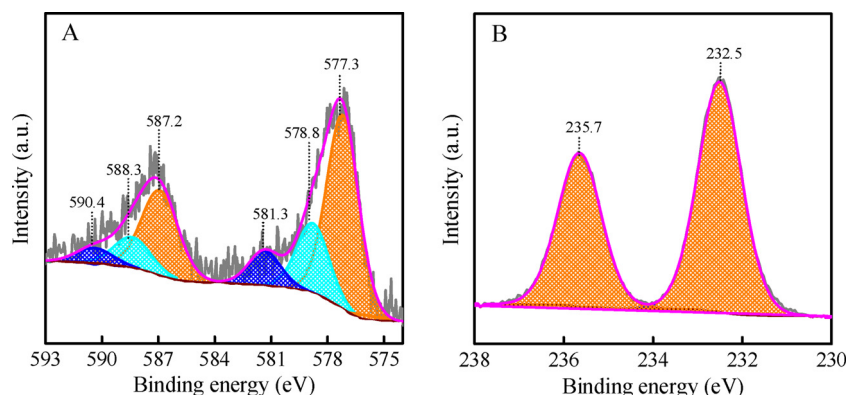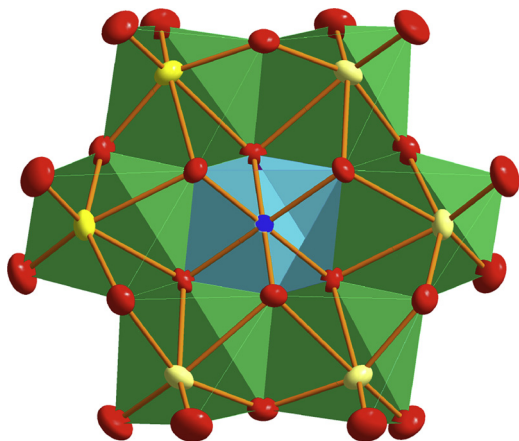
**Fig. 2.** UV–vis spectrum of prepared $Na_3H_6CrMo_6O_{24}$ sample.



**Fig. 3.** XPS spectra of (A) Cr 2p and (B) Mo 3d for $Na_3H_6CrMo_6O_{24}$ sample. The grey line indicates the recorded signals.



**Scheme 1.** The Anderson-type diagram of the $CrMo_6$ polyoxometalate. The blue, saffron yellow, and red balls represent Cr, Mo, and O atoms, respectively. (For interpretation of the references to colour in this scheme legend, the reader is referred to the web version of this article.)

Prevailingly, the stronger conductivity contributed to larger ions mobility in the liquid [40]. Consequently, this experiment result revealed that the ions migration rate in PEG/SSA was significantly better than that in other ones, which would be likely benefit the following catalytic performance in terms of the substance contact in the catalytic system.

On the other hand, the composition of DESs greatly affected their viscosity, which was also related to ions mobility rates in the liquid phase [40,41]. As illustrated in Fig. 4B, the viscosity of PEG/SSA DES was minimum (PEG/SSA, 255.6 mPa·S) in comparison with that of other five ones (PEG/DL-MA, 374.2 mPa·S; PEG/OXA, 381 mPa·S; PEG/DHBA, 360 mPa·S; PEG/PAS, 392.6 mPa·S; PEG/SA, 350.4 mPa·S). It implied that the weak shearing strength was formed in PEG/SSA,

further resulting in the strong ions migration rate under suitable condition. Combined with conductivity analyses, it was concluded that PEG/SSA DES system possessed maximum conductivity and minimum viscosity by comparing with other DESs systems. Herein, a factor (denoted as $C_v$, $C_v$ = conductivity/viscosity) of a certain DES system was defined for the convenient description in the following parts and being correlated with desulfurization performance. The $C_v$ value was shown in the following sequence of PEG/SSA (0.198) > > PEG/SA (0.0198) > PEG/DL-MA (0.0063) > PEG/OXA (0.0052) ≈ PEG/DHBA (0.005) ≈ PEG/PAS (0.0049).

Every kind of DES in this manuscript was derived from mixing PEG with organic acid under mild conditions. In the case of PEG/SSA DES, the FT-IR spectra were used to detect the interaction between PEG and SSA (Fig. 5). The bands at approximate 1039, 1167, and 1227 $cm^{-1}$ in SSA, assigned to stretch vibration of -$SO_3H$ group [42], were obviously observed. PEG demonstrated the C−O stretching band at about 1115 $cm^{-1}$ [42]. After the formation of PEG/SSA DES, the redshift of C−O band from 1115 to 1102 $cm^{-1}$ occurred, meanwhile this peak became more broad comparing with that of PEG. These results suggested that the hydrogen bond between PEG and SSA might be formed, leading to be complex for C−O micro-environment.

### 3.3. Screening of DESs for DBT removal

It is well-established that the composition of DESs play a significant role on their catalytic performance [4,7,15,39]. Therefore, the desulfurization activity of different DESs was evaluated using the DBT in decalin as the model diesel. The whole desulfurization process consisted of two stages, extraction (EDS) and aerobic oxidation (EAODS). It should be highlighted that this desulfurization process was carried out at the temperature of 60 °C with atmospheric pressure using $O_2$ as oxidation. This reaction conditions were more mild than these of other desulfurization systems reported previously, avoiding relatively high
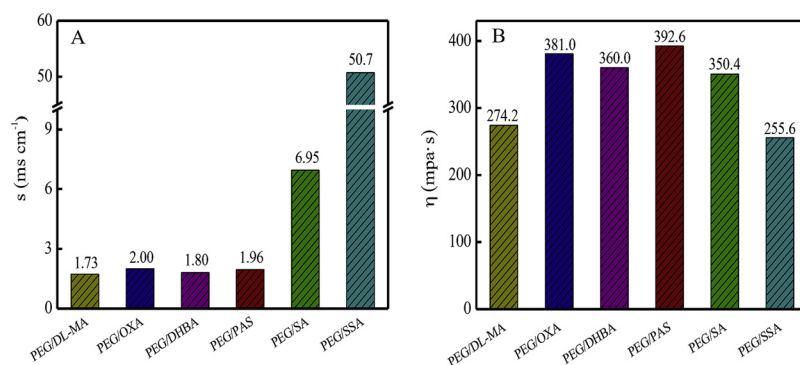
**Fig. 4.** (A) Conductivity and (B) viscosity of different DESs prepared from PEG and various organic acids measured at 60 °C.
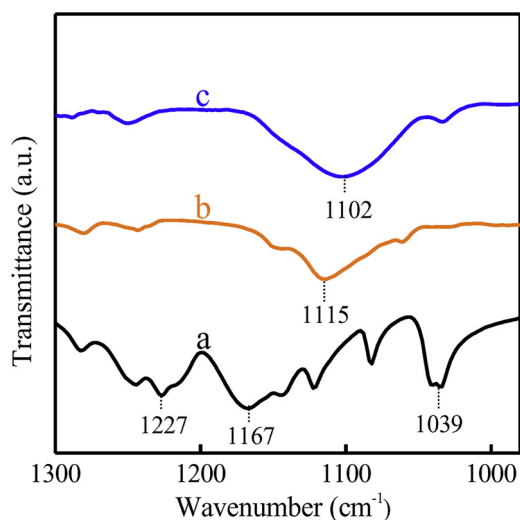


**Fig. 5.** FT-IR spectra of SSA (a), PEG (b), and PEG/SSA DES (c), respectively.

temperature and pressure [16,17,20]. As exhibited in Table 1, to illustrate the effect of DES, control experiments were also tested (Nos. 1–6). It was found that once PEG was added into this system, the EDS and EAODS were sharply increased. Otherwise the sulfur removal nearly didn't proceed. On the other hand, PEG and various organic acids containing different functional groups ($-SO_3H$, $-COOH$, $-NH_2$, and $-OH$) were utilized as HBA and HBD, respectively. It is as long as PEG was introduced into the desulfurization system that the S removal for EDS reached a same level (Nos. 4–12), indicating that DBT extraction process was mainly associated with the existence of PEG. When $CrMo_6$ was added, the DBT removal increased from 24 to 100% (Nos. 5 and 7). Without the addition of $O_2$, the oxidation desulfurization was also not carried out (No. 6). Moreover, except for PEG/SSA DES, the DBT removal in EDS was approximately equal to that in EAODS for other DESs, unravelling that the extraction process achieved equilibration within 30 min and the catalytic oxidation desulfurization process was almost not performed for these systems. Note that only PEG/SSA DES with $-SO_3H$ group possessed complete sulfur removal (100%) compared with other DESs (below 30%). At this point, it was inferred that the outstanding sulfur removal was mainly attributed to the synergistic effect of $CrMo_6$ polyoxometalate and DESs containing $-SO_3H$

**Table 1**
Effect of different desulfurization systems on the removal of DBT.

| No. | Name | HBA | HBD | Catalyst (g) | Reaction time (h) | Sulfur removal (%) | |
|-----|------|-----|-----|--------------|-------------------|---------------------|--|
| | | | | | | EDS[c] | EAODS[d] |
| 1 | — | — | — | — | 4 | 0 | 0 |
| 2 | — | — | — | 0.02 | 4 | 0 | 3 |
| 3 | SSA | — | | — | 4 | 0 | 1 |
| 4 | PEG | | — | — | 4 | 25 | 25 |
| 5 | PEG/SSA[a] | | | — | 4 | 23 | 24 |
| 6 | PEG/SSA[b] | | | 0.02 | 2 | 25 | 26 |
| 7 | PEG/SSA | | | 0.02 | 2 | 25 | 100 |
| 8 | PEG/SA | | | 0.02 | 2 | 25 | 30 |
| 9 | PEG/PAS | | | 0.02 | 2 | 26 | 28 |
| 10 | PEG/DHBA | | | 0.02 | 2 | 27 | 27 |
| 11 | PEG/OXA | | | 0.02 | 2 | 25 | 26 |
| 12 | PEG/DL-MA | | | 0.02 | 2 | 25 | 25 |

[a] The molar amounts of PEG and SSA were equal.
[b] Without the addition of $O_2$.
[c] Indicating extraction process. Extraction conditions: model diesel (S content of 500 ppm), 20 mL; DES if added, 4 mL; temp., 60 °C; time, 30 min.
[d] Indicating catalytic step after extraction. Reaction conditions: model diesel (S content of 500 ppm), 20 mL; DES if added, 4 mL; $CrMo_6$ if added, 0.02 g; temp., 60 °C; $O_2$ pressure, 1 atm.; flow rate of $O_2$, 60 mL min.
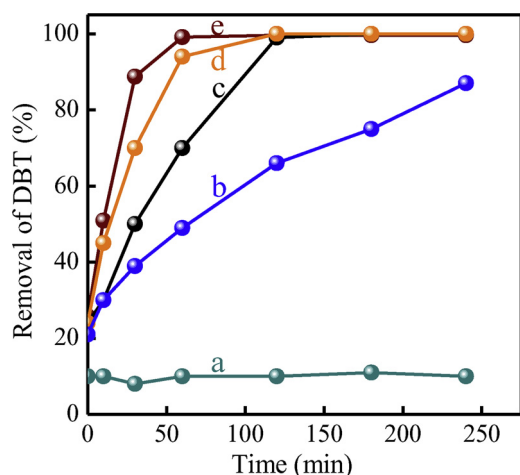
**Fig. 6.** Dependence of DBT removal on the reaction time at the temperature of 40 °C (a), 50 °C (b), 60 °C (c), and 70 °C (d), respectively. Reaction conditions: model diesel (S content of 500 ppm), 20 mL; DES, 4 mL; CrMo$_6$, 0.02 g; O$_2$ pressure, 1 atm.; flow rate of O$_2$, 60 mL min$^{-1}$.



**Fig. 7.** Dependence of DBT removal on the reaction time with model oil and DES volume ratio of 4 (a), 5 (b), 6 (c), 8 (d), 10 (e), and 20 (f), respectively. Reaction conditions: model diesel (S content of 500 ppm), 20 mL; CrMo$_6$, 0.02 g; O$_2$ pressure, 1 atm.; flow rate of O$_2$, 60 mL min$^{-1}$; temp., 60 °C.

group.

To further address the vital role of -SO$_3$H on the sulfur removal, the relationship between DBT removal and $C_v$ value mentioned above was correlated as illustrated in Fig. S2 (Supporting Information). As anticipated, with the $C_v$ value increasing, the DBT removal also enhanced. However, their relationship was not linear, unraveling that the $C_v$ value (conductivity/viscosity) was not the only influence factor and the intrinsic property of DES (*i.e.*, -SO$_3$H) was likely to dominate the catalytic oxidation process.

### 3.4. Sulfur removal performances

The sulfur removal performances were associated with not only materials themselves (extraction agent and catalyst) but also the reaction conditions [26,39]. In the following, temperature, time, and amounts of DES (namely, PEG/SSA) were investigated to obtain the optimal reaction conditions using DBT as the model substrate. Similarly, the removal system also proceeded at the mild temperature of below 70 °C with the oxidant of O$_2$ under atmospheric pressure.

The effect of temperature from 40 to 70 °C on DBT removal was shown in Fig. 6. Obviously, the DBT removal was improved with the increase of reaction time except for 40 °C. At 40 °C, the finding of low DBT removal (under 20%) in the extraction stage was probably due to the fact that existing state of DES in the form of solid at 40 °C led to the poor contact between DES and model oil. Additionally, the DBT removal almost maintained constant during the whole EAODS, indicating the catalytic oxidation process of DBT nearly didn't proceed at this temperature. Subsequently, with enhancing the temperature from 40 to 80 °C, the DBT removal during EDS (at 0 min) were increased and then kept constant. Nonetheless, the reaction rate for EAODS process were greatly improved, which was so fast that the DBT was almost completely transformed within 2 h at 60–80 °C. On basis of the reaction data from 50 to 80 °C and Arrhenius equation, the apparent activation energy of this oxidation desulfurization process was determined to be 33.9 kJ mol$^{-1}$ (Fig. S3). Given the sulfur removal activity and energy-consumption, the 60 °C was selected as the optimal temperature.

As depicted in Fig. 7, when the volume ratios of model oil to DES were ranged from 4 to 20, the removal of extraction desulfurization gradually decreased (at 0 min). It was reasonable that the more amount of DES was capable to facilitate the extraction removal of DBT. During the EAODS process, with the reaction time increasing, the DBT removal also enhanced but the increased degree varied for discrepant amount of DES contents. At $V_{oil}/V_{DES} = 20$, the desulfurization rate was so low
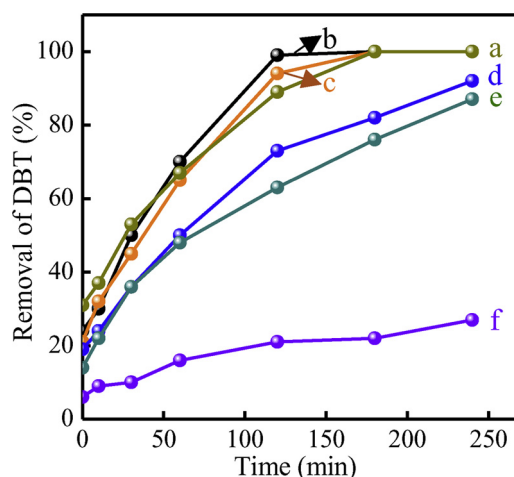
that the DBT removal achieved only 27% at 4 h. Subsequently, with the decrease of $V_{oil}/V_{DES}$ from 20 to 5, the DBT removal was always improved from 21% to 100% at 2 h. Whereas, further lowering the $V_{oil}/V_{DES}$ to 4, the decrease of DBT removal was observed, likely attributed to the relatively low concentration of DBT derived from the dilution effect of DES [43]. Thus, the volume ratio of model oil to DES was fixed to 5 in the following experiments. Additionally, 60 mL/min was chosen as the optimal O$_2$ flow rate (Fig. S4).

As can be seen from above DBT removal performances (Table 1, Figs. 6 and 7), this DES system coupled with CrMo$_6$ polyoxometalate demonstrated excellent desulfurization performances. To further illustrate the advantage of this coupled system, the scope of reaction substrate was extended to BT and 4,6-DMDBT (Fig. 8). Obviously, the 4,6-DMDBT removal was inferior to BT and DBT removal in the initial extraction stage, mainly derived from the steric effect of −CH$_3$ substituted group [42,43]. However, with catalytic reaction proceeding, the sulfur removal was shown in the sequence of DBT > 4,6-DMDBT > BT at 2 h. The S electron density in 4,6-DMDBT and DBT was higher than that in BT. It was generally accepted that the higher S electron density contributed to better removal activity under identical conditions [44]. Therefore, the removal of DBT and 4,6-DMDBT was superior
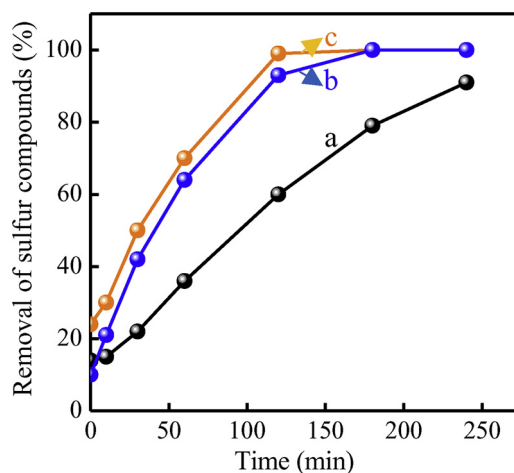


**Fig. 8.** Dependence of BT (a), 4,6-DMDBT (b), and DBT (c) removal on the reaction time. Reaction conditions: model diesel (S content of 500 ppm), 20 mL; DES, 4 mL; CrMo$_6$, 0.02 g; O$_2$ pressure, 1 atm.; flow rate of O$_2$, 60 mL min$^{-1}$; temp., 60 °C.

to that of BT. On the other hand, the steric effect of $-CH_3$ group in 4,6-DMDBT hindered its catalytic performance, giving rise to be inferior to S removal activity of DBT [45]. These experiment phenomena strongly supported the fact that sulfide removal was intensively affected by electron density and steric effect, in good agreement with previous reports from other catalytic systems such as titanosilicate and polyoxometalate [46,47]. Thus, this sulfide removal system coupling DESs with $CrMo_6$ polyoxometalate was also efficiently suitable for other large-sized S-containing organics like 4,6-DMDBT as well as BT with small molecular size under extremely mild condition (60 °C, atmospheric pressure, and $O_2$ as the oxidant).

The reusability of catalytic system is a vital issue, which determines their usability to practical applications [20,48]. After the first reaction for DBT removal, the flask with reaction system was transferred into refrigerator to dissociate the DES and oil phase overnight. Then the upper oil phase was collected using decantation method. The lower DES phase, containing DES, $CrMo_6$, and products, was performed using rotary evaporator to eliminate a minute amount of water derived from catalytic process. Subsequently, fresh model oil was again added into the above-mentioned DES to carry out the second run. As demonstrated in Fig. 9, the DBT in the model diesel was almost completely removed within 180 min before the fifth recycle. Meanwhile the initial reaction rates were approximately equal to $0.113$ mmol $L^{-1}$ min$^{-1}$. For the fifth run, the DBT removal and initial reaction rate were slightly decreased to 94% within 180 min and $0.068$ mmol $L^{-1}$ min$^{-1}$, respectively. The decrease of DBT removal may result from the transformation of crystal structure (see Fig. S5). At 240 min, the removal of DBT nearly achieved 100%. It was confirmed that this innovate desulfurization system was relatively stable and recyclable under extremely mild conditions.

Taking consideration of the outstanding desulfurization performance and greenization process, this system was further adopted to sulfur removal of commercially available diesel, including Commercial Diesel I and II. Due to the complexity of commercial diesel, micro-coulometry and GC-FPD were employed to quantitative and qualitative analyses of sulfur contents, respectively. With respect to Commercial Diesel I, it mainly consisted of BT, DBT, and their derivatives with the initial total S content of 242 ppm (Fig. 10A). After the first EAODS, these peaks ascribed to DBTs, nearly disappeared, while the BTs-related bands sharply decreased. It was inferred that the DBTs was much easier to remove by comparing with BTs, which was consistent with the results as shown in Fig. 8. Correspondingly, the total S content was lowered from 242 to 76 ppm (Fig. 10Ab). When the second cycle of EAODS proceeded, the sulfides were decreased to 21 ppm. For Commercial Diesel II (Fig. 10B), it possessed the initial sulfur content of

24 ppm, which mainly contained DBT and its derivatives. After only one cycle of EAODS, the total S content was tremendously reduced to 4 ppm, achieving the state of deep desulfurization. These results strongly confirmed that the present catalytic system coupling DESs with $CrMo_6$ polyoxometalate was a robust strategy for desulfurization *via* a green route.

### 3.5. Desulfurization mechanism

Numerous desulfurization technique has been reported in the literatures previously, containing extraction [9], oxidation [3,4,47], and adsorption et al [1]. To further investigate this desulfurization, time-dependent sulfur contents in both upper oil phase and below DES phase in the desulfurization system were analyzed (Fig. 11) and corresponding organics were identified by GC–MS (Figs. S6 and S7). After the reaction for DBT removal, the flask with reaction system was transfered into refrigerator to dissociate the DES and oil phase overnight. Then the upper oil phase was collected using decantation method, which was directly subjected to following measurements. The subjacent DES phase was added a certain amount of trichloromethane to make it homogeneous. As illustrated in Fig. 11, the sulfur content in the upper oil phase decreased from 54.3 to 40.7 μmol and simultaneously, that in the subjacent phase increased from 0 to 13.6 μmol during the extraction process of initial 30 min. It was speculated that the sulfide was migrated from upper to subjacent phase, derived from the extraction effects of DES. Subsequently, with the introduction of $CrMo_6$ polyoxometalate and oxidation of $O_2$, the S-content in oil phase continuously decreased and finally disappeared completely at 150 min, namely, after the catalytic reaction of 120 min, in well line with the results of GC–MS (Fig. S6, Supporting Information). Thus, the DBT was fully removed in this model oil, affording complete desulfurization. With respect to DES phase, at 90 min, both the DBT and dibenzothiophene sulfone existed at the same time (Fig. S7a, Supporting Information). The amount of S-containing compounds in the DES phase gradually rised, up to 54.2 μmol ultimately (dibenzothiophene sulfone, shown in Fig. S7b). These results indicated that the DBT in upper oil phase was extracted to subjacent DES phase, and catalytically oxidized with the assistance of $CrMo_6$ and $O_2$, which followed the EAODS process, as graphically illustrated in Scheme 2.

From Table 1, the conclusion of the synergistic effect of $CrMo_6$ polyoxometalate and DES in the sulfur removal have been made. To further shed light on how to cooperate for $CrMo_6$ and DES, UV–vis and FT-IR spectra of $CrMo_6$, DES, and their mixture were performed. As exhibited in Fig. 12A, a broad band centred at approximate 256 nm was observed for $CrMo_6$ without the $O_2$ treatment, while DES didn't demonstrate this signal without the $O_2$ treatment. When DES or $CrMo_6$ was subjected to $O_2$ treatment, no significant differences were noticed in the UV–vis spectra compared with corresponding parent without the $O_2$ treatment (Figs. S8 and S9). It should be pointed that this peak at 256 nm disappeared completely for the mixture of $CrMo_6$ and DES after $O_2$ treatment, indicative of the strong interaction between $O_2$ and $CrMo_6$ with the assistance of DES.

As shown in the FT-IR spectra (Figs. S10 and S11, Supporting Information), $O_2$-treated samples exhibited similar spectra to homologous parents, which was consistent with the UV–vis results. When the mixture of $CrMo_6$ and DES was disposed by $O_2$ at 60 °C (Fig. 12Bc), a new weak absorption peak at 963 cm$^{-1}$, assigned to peroxopolyanion [49], appeared. This result implied that DES facilitated the interaction of $CrMo_6$ and $O_2$, giving rise to the formation of peroxypolyoxoanion. Compared with the spectrum of DES, the band at 1039 cm$^{-1}$, associated with -SO$_3$H group [42,50], for the mixture purged with $O_2$ almost disappeared. Meanwhile, the spectrum for the mixture also demonstrated other two new peaks at 1060 and 1148 cm$^{-1}$. It has been reported that organic peroxyacid was easily capable to oxidize sulfide under suitable conditions, forming corresponding sulfone [43,51,52]. Combined above analysis results with reaction data (Table 1), it was
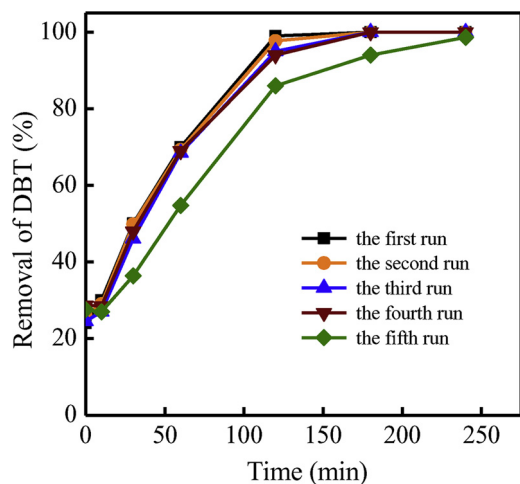
**Fig. 9.** Reusability of catalytic system in the removal of DBT. Reaction conditions: model diesel (S content of 500 ppm), 20 mL; DES, 4 mL; $CrMo_6$, 0.02 g; $O_2$ pressure, 1 atm.; flow rate of $O_2$, 60 mL min$^{-1}$; temp., 60 °C.
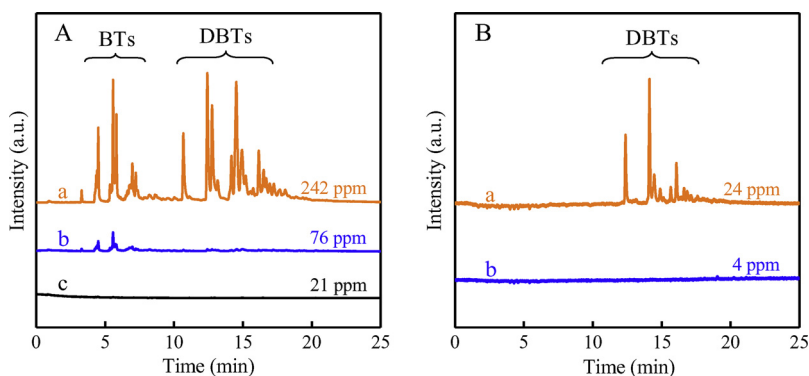
**Fig. 10.** Specific sulfur-containing GC-FPD spectra of initial sulfur contents (a), the first EAODS (b), and the second EAODS (c) process for commercial diesel I (A) and (B) commercial diesel II. Reaction conditions: commercially available diesel, 10 mL; DES, 10 mL; CrMo$_6$, 0.02 g; O$_2$ pressure, 1 atm.; flow rate of O$_2$, 60 mL min$^{-1}$; temp., 60 °C; time, 4 h.
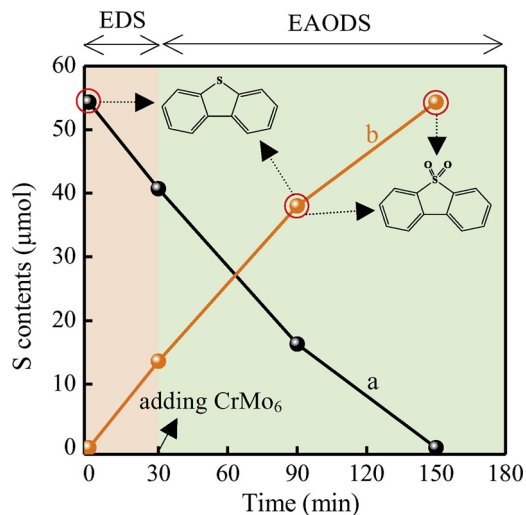


**Fig. 11.** Time-dependent sulfur contents in upper oil phase (a) and below DES phase (b).

speculated that this two bands were likely attributed to peroxy sulfonate. Additionally, the color of the CrMo$_6$ and DES mixture changed from light grey to saffron yellow after O$_2$ treatment (Fig. S12, Supporting Information). At this point, conclusion could be made that peroxypolyoxoanion was formed from CrMo$_6$ polyoxometalate with the aid of O$_2$ and DES, which then oxidized -SO$_3$H group in the DES to peroxysulfonic acid (also supported by selective quenching experiments in Fig. S13). This peroxyacid further selectively oxidized DBT with electron-rich S atoms into dibenzothiophene sulfone with the assistance of CrMo$_6$ (confirmed by Fig. S14), at the same time which was reduced to -SO$_3$H (Scheme 3). During the whole process, the CrMo$_6$ polyoxometalate and -SO$_3$H in DES played an important role of multistep electron transfer mediators and electron-donor, respectively, just like an enzymatically catalytic route (namely, biomimetic strategy) as graphically depicted in Schemes 2 and 3.

As a result, this biomimetic route obeyed the extraction and catalytically oxidative desulfurization process, during which multistep ETMs originated from the synergistic effect of CrMo$_6$ and DES were of significance for the sulfur removal with high efficiency.

## 4. Conclusions

A novel and biomimetic route coupling CrMo$_6$ polyoxometalate and PEG/SSA DES was proposed for oxidative desulfurization. This
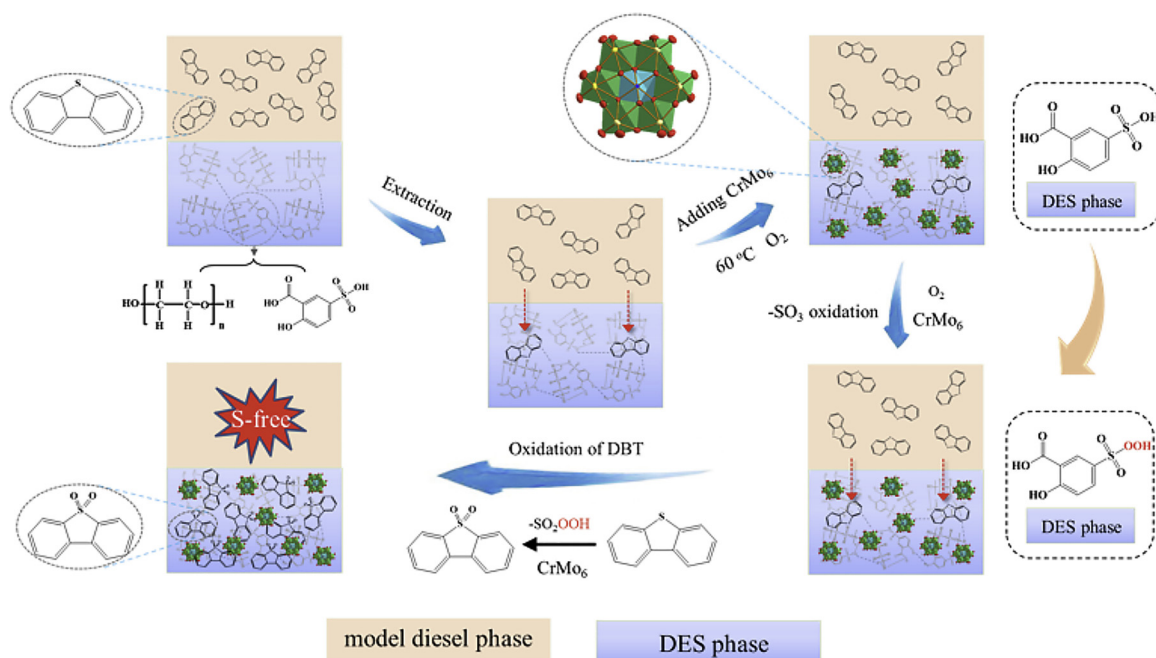


**Scheme 2.** Schematic representation of the proposed reaction mechanism for the oxidation desulfurization coupling CrMo$_6$ polyoxometalate with DESs.
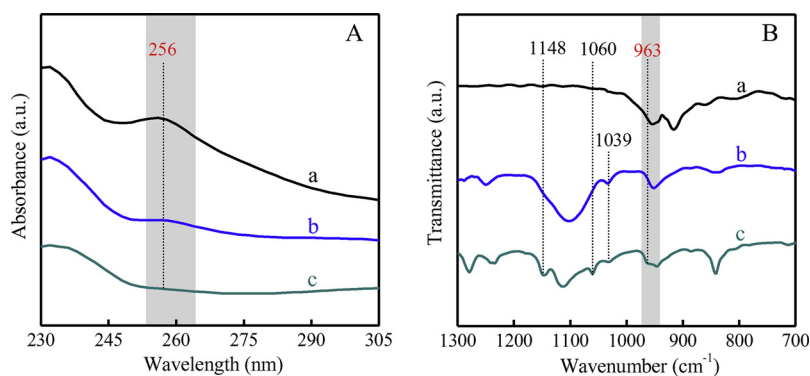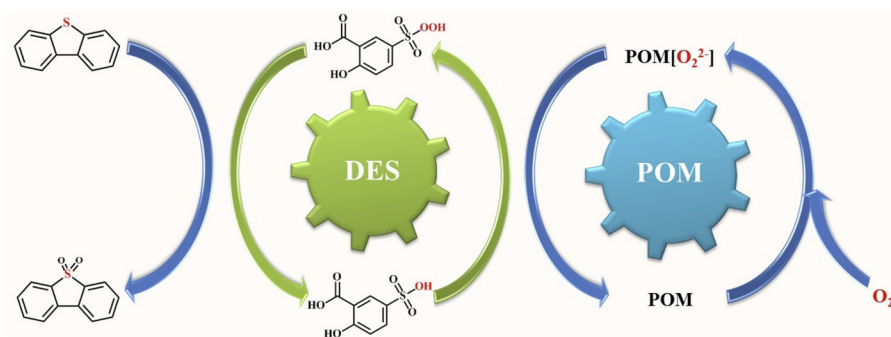
**Fig. 12.** UV–vis and FT-IR spectra of CrMo$_6$ polyoxometalate (a), DES (b), and the mixed sample of CrMo$_6$ and DES purged with O$_2$ (c). Note that the mixed sample of CrMo$_6$ and DES were disposed with O$_2$ at 60 °C for 1 h prior to FT-IR measurement.



**Scheme 3.** Proposed catalytic cycle for the biomimetic oxidative desulfurization.

desulfurization system demonstrated unique desulfurization performances at the extremely low temperature of 60 °C with ambient oxygen pressure. It has been confirmed that -SO$_3$H in the PEG/SSA DES played a significant role in removing sulfide. This desulfurization process followed the extraction-oxidation mechanism, during which DES and CrMo$_6$ POM severed as electron-donor and multistep electron transfer mediators, respectively, were two indispensable factors for highly efficient AODS. Moreover, the desulfurization activity without an obvious decrease was observed for DBT removal after four recycles. The deactivation of this catalytic system was likely derived from the transformation of CrMo$_6$ crystal structure. Thus, this biomimetic strategy provides an alternative and green route for constructing catalytic systems, which are performed under extremely mild conditions such as at room temperature with atmospheric pressure.

## Conflict of interest

The authors declare that they have no known competing financial interests or personal relationships that could have appeared to influence the work reported in this paper.

## Acknowledgment

## Appendix A. Supplementary data

Supplementary material related to this article can be found, in the online version, at doi:https://doi.org/10.1016/j.apcatb.2019.118089.

## References

[1] R.T. Yang, A.J. Hernández-Maldonado, F.H. Yang, Science 301 (2003) 79–81.
[2] A.J. Hernández-Maldonado, R.T. Yang, J. Am. Chem. Soc. 126 (2004) 992–993.
[3] G. Gao, S. Cheng, Y. An, X. Si, M. Fu, Y. Liu, H. Zhang, P. Wu, M. He, ChemCatChem. 2 (2010) 459–466.
[4] H. Lü, P. Li, C. Deng, W. Ren, S. Wang, P. Liu, H. Zhang, Chem. Commun. 51 (2015) 10703–10706.
[5] H. Lü, J. Gao, Z. Jiang, F. Jing, Y. Yang, G. Wang, C. Li, J. Catal. 239 (2006) 369–375.
[6] P.S. Kulkarni, C.A.M. Afonso, Green Chem. 12 (2010) 1139–1149.
[7] H. Xu, D. Zhang, F. Wu, X. Wei, J. Zhang, Fuel 225 (2018) 104–110.
[8] W. Zhou, Q. Wei, Y. Zhou, M. Liu, S. Ding, Q. Yang, Appl. Catal. B: Environ. 238 (2018) 212–224.
[9] P.S. Tam, J.R. Kittrell, J.M. Eldridge, Ind. Eng. Chem. Res. 29 (1990) 321–324.
[10] A. Pimerzin, A. Mozhaev, A. Varakin, M. Konstantin, P. Nikulshin, Appl. Catal. B: Environ. 205 (2017) 93–103.
[11] D. Solís, A.L. Agudo, J. Ramírez, T. Klimova, Catal. Today 116 (2006) 469–477.
[12] S.V. Chandra, RSC Adv. 2 (2012) 759–783.
[13] L. Hao, T. Su, D. Hao, C. Deng, W. Ren, H. Lü, Chin. J. Catal. 39 (2018) 1552–1559.
[14] A. Chica, G. Gatti, B. Moden, L. Marchese, E. Iglesis, Chem. Eur. J. 12 (2006) 1960–1967.
[15] L. Sun, T. Su, J. Xu, D. Hao, W. Liao, Y. Zhao, W. Ren, C. Deng, H. Lü, Green Chem. 21 (2019) 2629–2634, https://doi.org/10.1039/c8gc03941k.
[16] Y. Shi, G. Liu, B. Zhang, X. Zhang, Green Chem. 18 (2016) 5273–5279.
[17] W. Zhang, H. Zhang, J. Xiao, Z. Zhao, M. Yu, Z. Li, Green Chem. 16 (2014) 211–220.
[18] A. Gómez-Paricio, A. Santiago-Portillo, S. Navalón, P. Concepción, M. Alvaro, Green Chem. 18 (2016) 508–515.
[19] X. Zeng, X. Xiao, Y. Li, J. Chen, H. Wang, Appl. Catal. B: Environ. 209 (2017) 98–109.
[20] H. Lü, W. Ren, W. Liao, W. Chen, Y. Li, Z. Suo, Appl. Catal. B: Environ. 138–139 (2013) 79–83.
[21] H. Lü, Y. Zhang, Z. Jiang, C. Li, Green Chem. 12 (2010) 1954–1958.
[22] A.P. Abbott, G. Capper, D.L. Davies, R.K. Rasheed, V. Tambyrajah, Chem. Commun. 9 (2003) 70–71.
[23] N. Li, Y. Gao, X. Zhang, Z. Yu, L. Shi, Q. Sun, Chin. J. Catal. 36 (2015) 721–727.
[24] A. Shaabani, A.H. Rezayan, Catal. Commun. 8 (2007) 1112–1116.
[25] R. Ohkado, T. Ishikawa, H. Iida, Green Chem. 20 (2018) 984–988.
[26] J. Bäckvall, J. Piera, Angew. Chem. Int. Ed. 47 (2008) 3506–3523.
[27] A. Perloff, Inorg. Chem. 9 (1970) 2228–2239.
[28] H. An, D. Xiao, E. Wang, J. Mol. Struct. 751 (2005) 184–189.
[29] A. Corma, L.T. Nemeth, M. Renz, S. Valencia, Nature 412 (2001) 423–425.
[30] D.M. Shi, F.X. Ma, C.J. Zhang, Z. Anorg. Allg. Chem. 634 (2008) 758–763.
[31] J. Dong, J. Hu, Y. Chi, Z. Lin, B. Zou, S. Yang, C.L. Hill, C.A. Hu, Angew. Chem. Int.

Ed. 56 (2017) 4473–4477.

[32] C.A. Ohlin, E.M. Villa, J.C. Fettinger, W.H. Casey, Angew. Chem. Int. Ed. 47 (2008) 8251–8254.

[33] S. Mortazavian, H. An, D. Chun, J. Moon, Chem. Eng. J. 353 (2018) 781–795.

[34] B. Wichterlova, L. Krajcikova, Z. Tvaruzkova, J. Chem. Soc. 80 (1984) 2639–2645.

[35] L. Wang, P. Yin, J. Zhang, J. Hao, C. Lv, F. Xiao, Y. Wei, Chem. Eur. J. 17 (2011) 4796–4801.

[36] L. Fang, B. Wu, I.M.C. Lo, Chem. Eng. J. 319 (2017) 258–267.

[37] E.R. Cooper, C.D. Andrews, P.S. Wheatley, P.B. Webb, P. Wormald, R.E. Morris, Nature 430 (2004) 1012–1016.

[38] F. Liu, J. Barrault, V.K. De Oliveira, F. Jérôme, ChemSusChem 5 (2012) 1223–1226.

[39] A.P. Abbott, D. Boothby, G. Capper, D.L. Davies, R.K. Rasheed, J. Am. Chem. Soc. 126 (2004) 9142–9147.

[40] I.M. Aroso, A. Paiva, R.L. Reis, J. Mol. Liq. 241 (2017) 654–661.

[41] F. Li, B. Wu, R. Liu, X. Wang, L. Chen, D. Zhao, Chem. Eng. J. 274 (2015) 192–199.

[42] W. Zhu, C. Wang, H. Li, P. Wu, S. Xun, W. Jiang, Z. Chen, Z. Zhao, H. Li, Green Chem. 17 (2015) 2464–2472.

[43] W. Jiang, L. Dong, W. Liu, T. Guo, M. Zhang, W. Zhu, H. Li, RSC Adv. 7 (2017) 55318–55325.

[44] C. Wang, Z. Chen, W. Zhu, Energy Fuels 31 (2017) 1376–1382.

[45] H. Lü, P. Li, Y. Liu, L. Hao, W. Ren, W. Zhu, C. Deng, F. Yang, Chem. Eng. J. 313 (2017) 1004–1009.

[46] H. Lü, S. Wang, C. Deng, W. Ren, B. Guo, J. Hazard. Mater. 279 (2014) 220–225.

[47] V. Hulea, F. Fajula, J. Bousquet, J. Catal. 198 (2001) 179–186.

[48] S. Kim, G. Park, M.H. Woo, G. Kwak, S.K. Kim, ACS Catal. 9 (2019) 2880–2892.

[49] J. Gao, Y. Chen, B. Han, Z. Feng, C. Li, N. Zhou, S. Gao, Z. Xi, J. Mol. Catal. A-Chem. 210 (2004) 197–204.

[50] L. Hao, M. Wang, W. Shan, C. Deng, W. Ren, Z. Shi, H. Lü, J. Hazard. Mater. 339 (2017) 216–222.

[51] J. Dou, H.C. Zeng, ACS Catal. 4 (2014) 566–576.

[52] L. Cai, S. Li, D. Yan, L. Zhou, F. Guo, Q. Sun, J. Am. Chem. Soc. 140 (2018) 4869–4876.